Nonlinear Dyn (2013) 74:849–867
DOI 10.1007/s11071-013-1010-9

ORIGINAL PAPER

Periodic and quasiperiodic galloping of a wind-excited tower under external excitation

Mohamed Belhaq · Ilham Kirrou · Lahcen Mokni

Received: 7 May 2013 / Accepted: 12 July 2013 / Published online: 17 August 2013

Abstract The galloping of tall structures excited by steady and unsteady wind may be periodic or quasiperiodic (QP) with amplitudes having the same order of magnitude. While the onset of periodic and QP galloping was studied, their control on the other hand has received less attention. In this paper, we conduct analytical study on the effect of a fast harmonic excitation on the onset of periodic and QP galloping in the presence of steady and unsteady wind. We consider the cases where the unsteady wind activates either external excitation, parametric one or both. A perturbation analysis is performed to obtain close expressions of QP solution and the corresponding modulation envelopes. We show that at various loading situations, the periodic and QP galloping onset is significantly influenced by the amplitude of the fast external excitation. In the case where the unsteady wind activates parametric excitation, the QP galloping occurs with higher frequency modulation compared to the case where the unsteady wind activates external excitation. In the case where external and parametric excitations are activated simultaneously, fast harmonic excitation eliminates bistability in the amplitude response and gives rise to a new small QP modulation envelope.

M. Belhaq (✉) · I. Kirrou · L. Mokni
Laboratory of Mechanics, University Hassan II,
Casablanca, Morocco
e-mail: mbelhaq@yahoo.fr

Keywords Quasiperiodic galloping · Wind effect · Structural dynamics · Perturbation analysis · Control · Fast excitation

1 Introduction

Dynamic analysis of tall structures under unsteady (turbulent) wind excitation has been a major concern in constructing and designing stable buildings. Indeed, wind-induced vibrations of such buildings may cause galloping above a certain threshold of the wind speed [1–5]. In this context, considerable efforts have been done to control the amplitude of such wind-induced vibrations; see, for instance, [6] in which a review of the main classes of semiactive control devices is given and their full-scale implementation to civil infrastructure applications is presented.

The effect of unsteady wind on periodic galloping of tall prismatic structures has been studied considering a lumped single degree of freedom (sdof) model [4]. The multiple scales method (MSM) was applied and the response of the system examined near primary and secondary resonances. The results shown that the unsteady wind decreases the wind speed onset (the critical wind speed above which galloping occurs) near the primary resonance and has no significant influence near secondary resonances. This study [4] has been extended to analyze the effect of self- and external or/and parametric excitations on periodic galloping of a tower near the primary resonance [7]. Using

the MSM, the effect of unsteady wind on Hopf bifurcation was analyzed and the influence of steady wind speed on QP response was reported based on numerical simulation.

In tall structures subjected to steady wind, Hopf bifurcation may occur at a critical wind speed. However, when a structure is under steady and unsteady wind, the induced motion of the structure may be periodic or QP [7]. The periodic galloping usually occurs around the resonance, while the QP one appears away from the resonance resulting from the interaction between self- and external or/and parametric excitations [8–11]. In this situation, the existence of periodic and QP responses may lead to frequency-locking (or synchronization) between the frequency of the unsteady force and the frequency of the self excitation. Such a mechanism is produced by the disappearance of a slow flow limit cycle through a homoclinic or heteroclinic bifurcation [12–15].

Due to the fact that the amplitude of QP galloping of a tower is found to be of the same order of magnitude as that of the periodic response [7], the effect of wind speed on the onset of QP galloping should not be ignored and has to be taken into consideration and analyzed carefully. For instance, it was shown numerically using 3D model that wind-excited large stress tower develops QP response rather than periodic oscillations [16]. Recently, the effect of wind speed on the onset of QP galloping has been examined analytically [17] and it was shown that QP galloping can occur even for small values of the wind velocity with amplitude having the same order of magnitude as that of periodic galloping.

In this paper, we extends the previous studies [4, 7, 17] by focusing principally on the effect of external fast harmonic excitation (FHE) on the periodic and QP galloping onset. Specifically, we conduct analytical treatment to approximate the QP response and its modulation envelope. Then we examine the effect of FHE on the onset of periodic and QP galloping in the presence of unsteady wind. The QP solutions and the modulation envelopes are obtained using the method of three stage perturbation analysis (TSPA) [18, 19], which consists of applying the method of direct partition of motion (DPM) [20–22] followed by two stages of MSM [23].

The paper is organized as follows: In Sect. 2, the equation of motion is given and the DPM followed by a first MSM are applied to derive the modulation equations of the slow dynamic near the primary resonance. In Sect. 3, we analyze the effect of the FHE amplitude on the periodic galloping onset in the cases where the unsteady wind activates either an external excitation, a parametric one or both. In Sect. 4, we apply a second MSM on the modulation equations to approximate the QP solutions and the QP modulation envelopes. A careful analysis is conducted to examine the effect of the FHE on QP galloping onset in the case of various loading situations. A summary of the results is provided in the concluding section.

2 Equation of motion and slow flow

A single mode approach of the structure motion is considered and modeled by a sdof lumped mass system [4, 7]. It is assumed that the tower is under steady and unsteady wind flow and suppose that a FHE can be introduced to excite the structure. In this case, the dimensionless sdof equation of motion can be written in the form [7]

$$\ddot{x} + x + \left[c_a(1-\bar{U}) - b_1 u(t)\right]\dot{x} + b_2\dot{x}^2 + \left[\frac{b_{31}}{\bar{U}} + \frac{b_{32}}{\bar{U}^2}u(t)\right]\dot{x}^3 = \eta_1\bar{U}u(t) + \eta_2\bar{U}^2 + Y\cos\nu t \tag{1}$$

where the dot denotes differentiation with respect to the nondimensional time t. Equation (1) contains, in addition to the elastic, viscous, and inertial linear terms, quadratic and cubic components in the velocity generated by the aerodynamic forces. The steady component of the wind velocity is represented by $\bar{U}$ and the turbulent wind flow is approximated by a periodic force, $u(t)$, which is assumed to include the two first harmonics, $u(t) = u_1 \sin\Omega t + u_2 \sin 2\Omega t$, where u_1, u_2 and Ω are, respectively, the amplitudes and the fundamental frequency of the response. We shall analyze the case of external excitation ($u_1 \neq 0, u_2 = 0$), the case of parametric one ($u_1 = 0, u_2 \neq 0$), and the case where external and parametric excitations are present simultaneously. The coefficients of Eq. (1) and numerical values of parameters are given in Appendix A and Y, ν are the amplitude and the frequency of the fast excitation, respectively. Notice that the case of two towers linked by a nonlinear viscous device submitted to turbulent wind flow has been considered in [24].

The introduction of a FHE as a possible control strategy was motivated by a previous experimental

work done for vibrating testing purpose of a full size tower [25]. The mechanical vibration exciter system used in such an experiment consists of a pair of counter-rotating eccentric weights so arranged that a rectilinear sinusoidally varying horizontal inertia force is generated. The two weights rotate about a common vertical shaft, and are driven in opposite directions by a chain-drive system. This vibration exciter is placed on the top of the structure and debits a harmonic force able to excite the structure. Here, we assume that the generated frequency of the vibration exciter is relatively higher than the natural frequency of the first mode of the tower such that the other lower modes of the tower cannot be activated.

Equation (1) includes a slow dynamic due to the steady and unsteady wind and a fast dynamic induced by the FHE. To examine the influence of the FHE on periodic and QP galloping, we first perform the method of DPM, which consists in introducing two different time scales, a fast time $T_0 = \nu t$ and a slow time $T_1 = t$, and splitting up $x(t)$ into a slow part $z(T_1)$ and a fast part $\phi(T_0, T_1)$ as

$$x(t) = z(T_1) + \mu\phi(T_0, T_1) \tag{2}$$

where z describes the slow main motions at time-scale of oscillations, $\mu\phi$ stands for an overlay of the fast motions and μ indicates that $\mu\phi$ is small compared to z. Since ν is considered as a large parameter, we choose $\mu \equiv \nu^{-1}$ for convenience. The fast part $\mu\phi$ and its derivatives are assumed to be 2π-periodic functions of fast time T_0 with zero mean value with respect to this time, so that $\langle x(t)\rangle = z(T_1)$ where $\langle\rangle \equiv \frac{1}{2\pi}\int_0^{2\pi}()\,dT_0$ defines time-averaging operator over one period of the fast excitation with the slow time T_1 fixed. Averaging procedure gives the following equation governing the slow dynamic of motion:

$$\begin{aligned}\ddot{z} + z + \Bigg[c_a(1-\bar{U}) - b_1 u(t) &+ H\left(\frac{b_{31}}{\bar{U}} + \frac{b_{32}}{\bar{U}^2}u(t)\right)\Bigg]\dot{z} + b_2\dot{z}^2 \\ &+ \left[\frac{b_{31}}{\bar{U}} + \frac{b_{32}}{\bar{U}^2}u(t)\right]\dot{z}^3 \\ &= -G + \eta_1\bar{U}u(t) + \eta_2\bar{U}^2\end{aligned} \tag{3}$$

where $H = \frac{3Y^2}{2\nu^2}$ and $G = -\frac{b_2Y^2}{2\nu^2}$. Details on the averaging procedure and the derivation of the slow dynamic (3) are given in Appendix B. Note that the case without fast excitation ($Y = 0$ or $H = G = 0$) was considered in [7]. To obtain the modulation equations of the slow dynamic (3) near primary resonance, the MSM was performed by introducing a bookkeeping parameter ε, scaling as $z = \varepsilon^{\frac{1}{2}}z$, $b_1 = \varepsilon b_1$, $b_2 = \varepsilon^{\frac{1}{2}}b_2$, $\eta_1 = \varepsilon^{\frac{3}{2}}\eta_1$, $\eta_2 = \varepsilon^{\frac{3}{2}}\eta_2$, and assuming that $\bar{U} = 1 + \varepsilon V$ (V stands for the mean wind velocity) and the resonance condition $\Omega = 1 + \varepsilon\sigma$ where σ is a detuning parameter [7]. Scaling also $H = \varepsilon H$, a two-scale expansion of the solution is sought in the form

$$z(t) = z_0(t_0, t_1) + \varepsilon z_1(t_0, t_1) + O\left(\varepsilon^2\right) \tag{4}$$

where $t_i = \varepsilon^i t$ $(i = 0, 1)$. In terms of the variables t_i, the time derivatives become $\frac{d}{dt} = d_0 + \varepsilon d_1 + O(\varepsilon^2)$ and $\frac{d^2}{dt^2} = d_0^2 + 2\varepsilon d_0 d_1 + O(\varepsilon^2)$, where $d_i^j = \frac{\partial^j}{\partial^j t_i}$. Substituting Eq. (4) into Eq. (3), equating coefficients of the same power of ε, we obtain the two first orders

$$d_0^2 z_0 + z_0 = -G \tag{5}$$

$$\begin{aligned}d_0^2 z_1 + z_1 = &-2d_0d_1z_0 + \big(c_aV + b_1u(t_0) \\ &- H\big(b_{31} + b_{32}u(t_0)\big)\big)(d_0z_0) \\ &- b_2(d_0z_0)^2 \\ &- \big(b_{31} + b_{32}u(t_0)\big)(d_0z_0)^3 \\ &+ \eta_1u(t_0) + \eta_2\end{aligned} \tag{6}$$

A solution to the first order of system (5) is given by

$$z_0 = A(t_1)\exp(it_0) + \bar{A}(t_1)\exp(-it_0) - G \tag{7}$$

where i is the imaginary unit and A is an unknown complex amplitude. Equation (6) can be solved for the complex amplitude A by introducing its polar form as $A = \frac{1}{2}ae^{i\phi}$. Substituting the expression of A into Eq. (6) and eliminating the secular terms, the modulation equations of the amplitude a and the phase ϕ can be extracted as

$$\begin{cases}\dot{a} = \big[S_1 - S_3\sin(2\phi)\big]a + \big[-S_2 + 2S_4\sin(2\phi)\big]a^3 \\ \qquad - \beta\cos(\phi) \\ a\dot{\phi} = \big[\sigma - S_3\cos(2\phi)\big]a + \big[S_4\cos(2\phi)\big]a^3 \\ \qquad + \beta\sin(\phi)\end{cases} \tag{8}$$

where $S_1 = \frac{1}{2}(c_aV - Hb_{31})$, $S_2 = \frac{3}{8}b_{31}$, $S_3 = \frac{1}{4}(b_1 - Hb_{32})u_2$, $S_4 = \frac{b_{32}}{8}u_2$, and $\beta = \frac{\eta_1u_1}{2}$. It is interesting to observe from the latter expressions that the FHE influences the dynamic of the tower through the parameter

H ($=\frac{3Y^2}{2\nu^2}$) introduced into the coefficients S_1 and especially S_3 which is related to the parametric excitation u_2.

3 Periodic galloping

In this section, we report on the effect of the amplitude of the FHE on the galloping of tower. To be consistent with previous results, the numerical values used here are picked from [7]. Periodic solutions of Eq. (3) corresponding to equilibria of the slow flow (8) are given by setting $\dot{a} = \dot{\phi} = 0$ in (8). We obtain a trivial solution $a = 0$ and a nontrivial one

$$a = \sqrt{\frac{4(c_a V - H b_{31})}{3 b_{31}}} \tag{9}$$

which corresponds to the periodic galloping amplitude of the tower. Figure 1 shows the galloping amplitude a versus the wind velocity V in the absence of the unsteady wind ($u_1 = 0, u_2 = 0$) and for different values of the FHE amplitude Y. Hereafter, the frequency of the FHE will be fixed, $\nu = 8$. This value of the frequency is chosen such that other modes of the tower are not excited. Figure 1 shows that increasing the amplitude of the FHE retards substantially the galloping onset. Instead, in the absence of FHE increasing the amplitude of the unsteady wind component decreases rapidly the galloping onset [4, 7].

In the case of turbulent wind with external excitation ($u_1 \neq 0, u_2 = 0$), the amplitude-response equation obtained from the slow flow (8) reads

$$S_2^2 a^6 - 2 S_1 S_2 a^4 + \left(S_1^2 + \sigma^2\right) a^2 - \beta^2 = 0 \tag{10}$$

In Fig. 2, we show the effect of the amplitude Y on the galloping amplitude, as given by Eq. (10), for given values of the excitation u_1. The solid line corresponds to the stable branch, while the dashed line corresponds to the unstable one. The results of numerical simulations (circles) are obtained using the fourth-order Runge–Kutta method. One observes in Fig. 2a that the

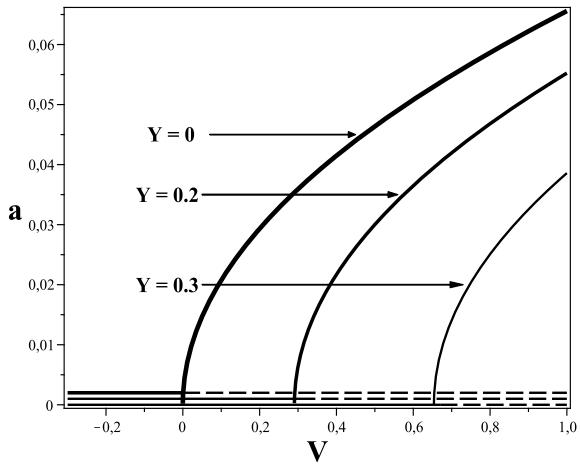

Fig. 1 Effect of the amplitude Y on galloping onset in the absence of turbulent wind ($u_1 = 0, u_2 = 0$). *Solid line*: stable; *dashed line*: unstable

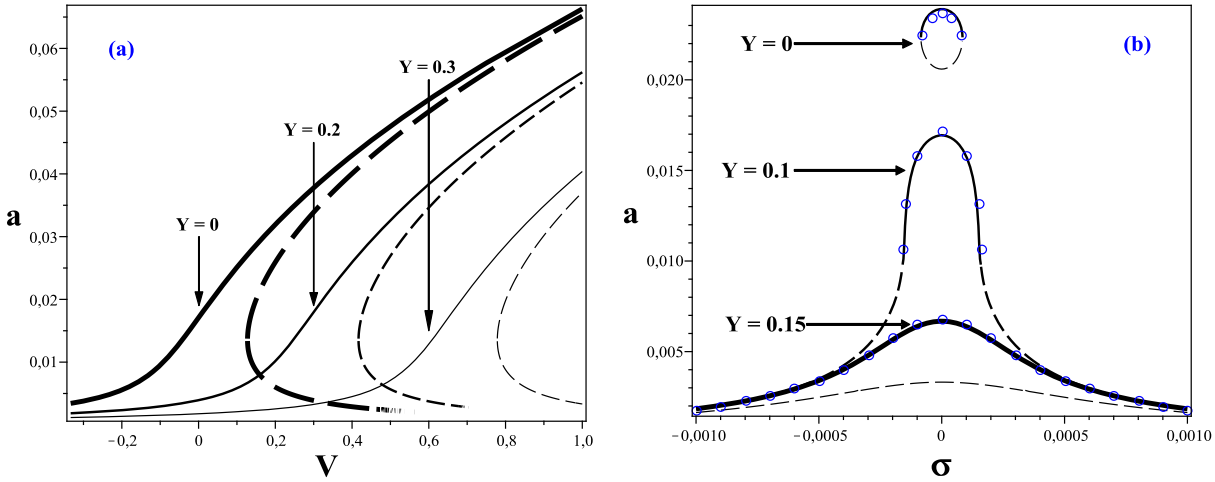

Fig. 2 Effect of Y on galloping amplitude; (**a**) $u_1 = 0.1, \sigma = 0$, (**b**) $u_1 = 0.033, V = 0.117$. *Solid line*: stable; *dashed line*: unstable; *circle*: numerical simulation

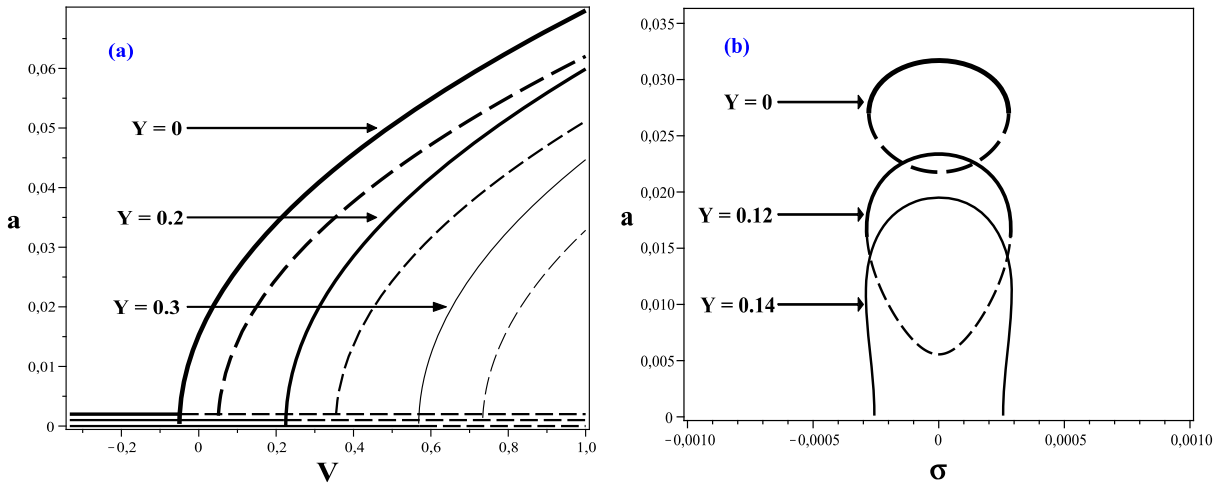

Fig. 3 Effect of Y on the galloping amplitude; (**a**) $u_2 = 0.1$, $\sigma = 0$, (**b**) $u_2 = 0.1$, $V = 0.167$. *Solid line*: stable; *dashed line*: unstable; *circle*: numerical simulation

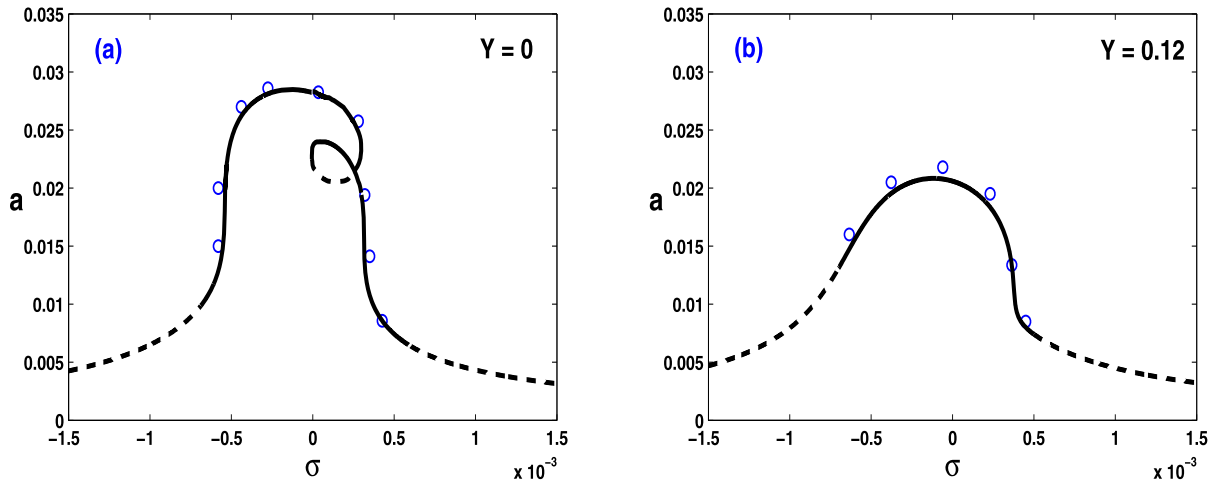

Fig. 4 Effect of Y on the periodic galloping; $V = 0.11$, $u_1 = 0.1$, $u_2 = 0.1$. *Solid line*: stable; *dashed line*: unstable; *circle*: numerical simulation

FHE increases the critical wind speed by shifting the galloping amplitude toward higher wind velocities resulting in a decrease of the corresponding amplitude for a given wind velocity V. Figure 2b shows the effect of the amplitude Y on the galloping versus σ indicating effectively that the galloping amplitude decreases with increasing Y.

In the case of turbulent wind with parametric excitation ($u_1 = 0, u_2 \neq 0$), the amplitude-response equation is given by

$$\frac{(-S_1 a + S_2 a^3)^2}{(-S_3 a + 2S_4 a^3)^2} + \frac{(-\sigma a)^2}{(-S_3 a + S_4 a^3)^2} = 1 \qquad (11)$$

Figure 3a shows, for a given value of the excitation u_2, the effect of the amplitude Y on the galloping amplitude versus the wind velocity V, as given by (11). A solid line corresponds to a stable branch and a dotted line corresponds to unstable one. It can be seen from this figure that in the absence of the fast excitation ($Y = 0$) the parametric component shifts the stable branch right. As a result, the value of the wind velocity V at which galloping occurs is decreased [4, 7]. Instead, a retarding effect of the galloping onset is achieved for increasing values of the FHE amplitude Y. Figure 3b shows the amplitude of the response

versus σ for different values of Y and for fixed V and u_2 indicating a decrease of the galloping amplitude as Y is increased.

In the case where the turbulent wind activates both external and parametric excitations ($u_1 \neq 0$, $u_2 \neq 0$), Figs. 4a, 4b show, respectively, the periodic amplitude in the absence and presence of the FHE amplitude Y. The comparison between the analytical predictions (solid lines) and the numerical simulations (circles) shows a good agreement. These figures indicate that increasing Y eliminates the bistability indicated by a loop in the amplitude response, which corresponds to the coexistence of two different amplitudes of (periodic) oscillation.

4 Quasiperiodic galloping

To approximate periodic solutions of the slow flow (8) corresponding to QP responses of the slow dynamic (3) we perform the third step of the TSPA. To this end one transforms the slow flow from the polar form (8) to the following Cartesian system using the variable change $u = a\cos\phi$ and $v = -a\sin\phi$

$$\begin{cases} \dfrac{du}{dt} = (\sigma + S_3)v - \beta \\ \qquad + \eta\{S_1 u - (S_2 u + S_4 v)(u^2 + v^2) \\ \qquad - 2S_4 u^2 v\} \\ \dfrac{dv}{dt} = -(\sigma - S_3)u \\ \qquad + \eta\{S_1 v - (S_2 v + S_4 u)(u^2 + v^2) - 2S_4 u v^2\} \end{cases} \tag{12}$$

where η is a new bookkeeping parameter introduced in damping and nonlinearity such that the unperturbed system of Eq. (12) has a basic solution (Eq. (14)). Following [18, 26, 27] by using the MSM, a periodic solution of the slow flow (12) can be sought in the following form:

$$\begin{aligned} u(t) &= u_0(T_1, T_2) + \eta u_1(T_1, T_2) + O\big(\eta^2\big) \\ v(t) &= v_0(T_1, T_2) + \eta v_1(T_1, T_2) + O\big(\eta^2\big) \end{aligned} \tag{13}$$

where $T_1 = t$ and $T_2 = \eta t$. Introducing $D_i = \frac{\partial}{\partial T_i}$ yields $\frac{d}{dt} = D_1 + \eta D_2 + O(\eta^2)$, substituting (13) into (12) and collecting terms, we get at different order of η

$$\begin{aligned} &D_1^2 u_0 + \lambda^2 u_0 = 0 \\ &\alpha v_0 = D_1 u_0 + \beta \end{aligned} \tag{14}$$

$$\begin{aligned} &D_1^2 u_1 + \lambda^2 u_1 \\ &\quad = \alpha\big[-D_2 v_0 + S_1 v_0 - (S_2 v_0 + S_4 u_0)\big(u_0^2 + v_0^2\big) \\ &\qquad - 2S_4 u_0 v_0^2\big] - D_1 D_2 u_0 + S_1 D_1 u_0 \\ &\qquad - D_1\big[(S_2 u_0 + S_4 v_0)\big(u_0^2 + v_0^2\big) + 2S_4 u_0^2 v_0\big] \\ &\quad \alpha v_1 = D_1 u_1 + D_2 u_0 - S_1 u_0 \\ &\qquad\qquad + (S_2 u_0 + S_4 v_0)\big(u_0^2 + v_0^2\big) + 2S_4 u_0^2 v_0 \end{aligned} \tag{15}$$

where $\alpha = \sigma + S_3$ and

$$\lambda = \sqrt{\sigma^2 - S_3^2} \tag{16}$$

defines the frequency of the periodic solution of the slow flow (12) corresponding to the frequency of the QP modulation. It should be noted that this frequency λ depends on the parametric excitation u_2 via the coefficient S_3 given in (8) indicating that the frequency of the QP modulation is influenced by the parametric excitation of the unsteady wind.

The solution of the first-order system (14) is given by

$$\begin{aligned} u_0(T_1, T_2) &= R(T_2)\cos\big(\lambda T_1 + \theta(T_2)\big) \\ v_0(T_1, T_2) &= -\frac{\lambda}{\alpha} R(T_2)\sin\big(\lambda T_1 + \theta(T_2)\big) + \frac{\beta}{\alpha} \end{aligned} \tag{17}$$

Substituting (17) into (15) and removing secular terms gives the following autonomous *slow slow* flow system on R and θ:

$$\begin{cases} \dfrac{dR}{dt} = \left(S_1 - 2\dfrac{\beta^2}{\alpha^2} S_2\right) R - \left(\dfrac{1}{2} S_2 + \dfrac{\lambda^2}{2\alpha^2} S_2\right) R^3 \\ R\dfrac{d\theta}{dt} = \left(\dfrac{3\beta^2}{2\alpha\lambda} S_4 - \dfrac{3\lambda\beta^2}{2\alpha^3} S_4\right) R \\ \qquad - \left(\frac{3\lambda^3}{8\alpha^3} S_4 - \frac{3\alpha}{8\lambda} S_4\right) R^3 \end{cases}$$

Thus, an approximate periodic solution of the slow flow (12) is given by

$$\begin{aligned} u(t) &= R\cos(\phi t) \\ v(t) &= -\frac{\lambda}{\alpha} R\sin(\phi t) + \frac{\beta}{\alpha} \end{aligned} \tag{18}$$

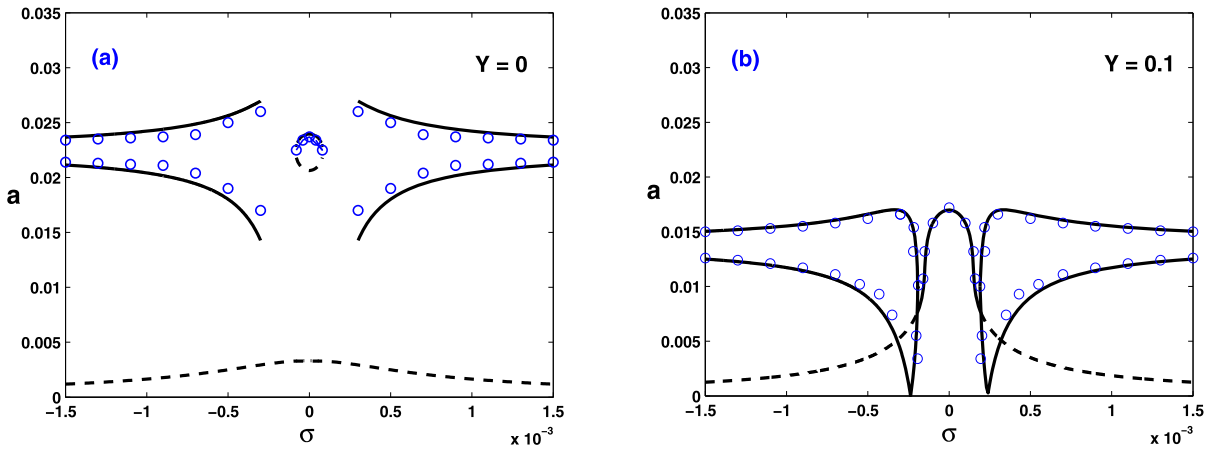

Fig. 5 Periodic and QP galloping versus σ for $V = 0.117$ and $u_1 = 0.033$. *Solid lines*: stable; *dashed lines*: unstable; *circle*: numerical simulation

where the amplitude R obtained by setting $\frac{dR}{dt} = 0$ is given by

$$R = \sqrt{\frac{2\alpha^2 S_1 - 4\beta^2 S_2}{S_2(\alpha^2 + \lambda^2)}} \tag{19}$$

and ϕ is given in Appendix B by Eq. (29).

Using (18) and (19), the modulated amplitude of the QP oscillations is approximated by

$$a(t) = \left\{\left[\frac{1}{2}R^2 + \frac{\lambda^2}{2\alpha^2}R^2 + \frac{\beta^2}{\alpha^2}\right] - \left[\frac{2\lambda\beta}{\alpha^2}R\sin(\phi) - \left(\frac{1}{2}R^2 - \frac{\lambda^2}{2\alpha^2}R^2\right)\cos(2\phi)\right]\right\}^{\frac{1}{2}} \tag{20}$$

and the QP envelope is delimited by $a_{\min}$ and $a_{\max}$ given, respectively, by

$$a_{\min} = \min\left\{\left[\left[\frac{1}{2}R^2 + \frac{\lambda^2}{2\alpha^2}R^2 + \frac{\beta^2}{\alpha^2}\right] \pm \frac{2\lambda\beta}{\alpha^2}R \pm \left(\frac{1}{2}R^2 - \frac{\lambda^2}{2\alpha^2}R^2\right)\right]\right\} \tag{21}$$

$$a_{\max} = \max\left\{\left[\left[\frac{1}{2}R^2 + \frac{\lambda^2}{2\alpha^2}R^2 + \frac{\beta^2}{\alpha^2}\right] \pm \frac{2\lambda\beta}{\alpha^2}R \pm \left(\frac{1}{2}R^2 - \frac{\lambda^2}{2\alpha^2}R^2\right)\right]\right\} \tag{22}$$

Using (21) and (22), the critical detuning parameter σ_c given by the conditions

$$\begin{cases} \sigma_c = S_3 \pm \sqrt{\frac{2\beta^2 S_2}{S_1}} \\ \sigma_c = \pm S_3 \end{cases} \tag{23}$$

defines the interval $[-\sigma_c, \sigma_c]$ within which the galloping amplitude is periodic. Outside this interval, the galloping amplitude is QP. One observes that in the case of external excitation ($u_2 = 0$), $S_3 = 0$ and in the case of parametric one ($u_1 = 0$), $\beta = 0$. These two cases will be highlighted below.

4.1 Case of turbulent wind with external excitation

Next, we explore the QP modulation envelope and the influence of the FHE on the QP galloping onset. When the tower is under external excitation ($u_1 \neq 0, u_2 = 0$), Figs. 5a, 5b show the QP modulation envelope, as given by Eqs. (21), (22), and the periodic amplitude response, as given by Eq. (10), for given values of V and u_1 and for two different values of the FHE amplitude Y. The comparison between the analytical predictions (solid lines) and the numerical simulations obtained by using Runge–Kutta method (circles) reveals that the analytical approach predict well the envelope of the QP modulation.

The effect of the amplitude Y on the QP envelope is shown in Fig. 6. One can observe that as Y is increased, the mean amplitude of the QP response reduces substantially, while the modulation envelope

moves away from the resonance region to disappear, as shown in Fig. 7.

Figure 8 presents examples of time histories of the slow dynamic $z(t)$ obtained by performing numerical simulation of Eq. (3) for some values of Y picked from Figs. 5, 6, and 7. In the absence of the FHE ($Y = 0$), Figs. 8a, 8b show, respectively, the periodic response for $\sigma = 0$ and the QP one for $\sigma = 5 \times 10^{-4}$. Figures 8c, 8d show, for $Y = 0.12$ and $Y = 0.14$, respectively, a QP response with a small amplitude and slight modulation (Fig. 8c) and a periodic response with small amplitude (Fig. 8d), which is coherent with the analytical predictions shown in Figs. 6 and 7b.

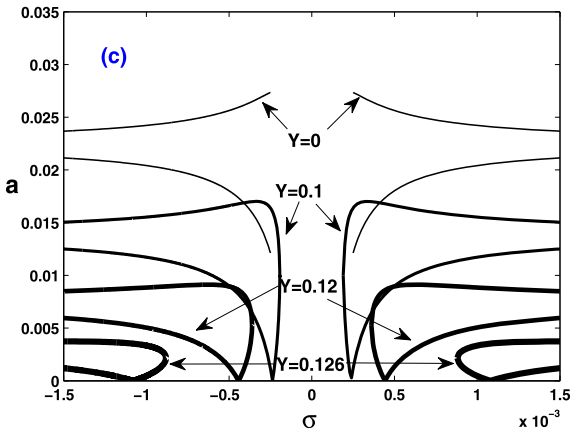

Fig. 6 QP galloping envelope versus σ for the parameter values of Fig. 5

Because the amplitude of the QP modulations is found to be of the same order of magnitude as that of the periodic response (Fig. 8), it is required that the QP galloping onset should be analyzed carefully. Based on Eq. (23), QP galloping may be expected mainly in certain region away from the resonance, as depicted in Figs. 5 and 7.

Figure 9a shows the QP envelope versus the wind velocity V for a given value of u_2 and in the absence of the FHE ($Y = 0$). For very small values of V, a small periodic response indicated by the horizontal line is observed, meaning that the tower always performs a small periodic oscillation due to the external excitation. As V is increased slightly, a small modulation of the periodic response appears (at the location where the horizontal line meets the QP envelope) giving rise to QP galloping onset. Increasing V further, the QP envelope delimited by $a_{\max}$ and $a_{\min}$ increases, as shown by time histories of the slow dynamic $z(t)$ inset Fig. 9a obtained by numerical simulation of Eq. (3).

Figure 9b shows the QP galloping amplitude in the presence of FHE. It can be seen that the FHE retards significantly the onset of QP galloping, keeping the tower oscillating periodically with small amplitude in large interval of the wind velocity indicated by the (thick) horizontal line. The boxes inset the figure show time histories before and after the QP galloping onset.

In Fig. 10, we show in the parameter plane σ_c versus V (Fig. 10a) and σ_c versus Y (Fig. 10b) the curves delimiting the regions of periodic (hatched) and QP galloping (unhatched), as given by Eq. (23). One ob-

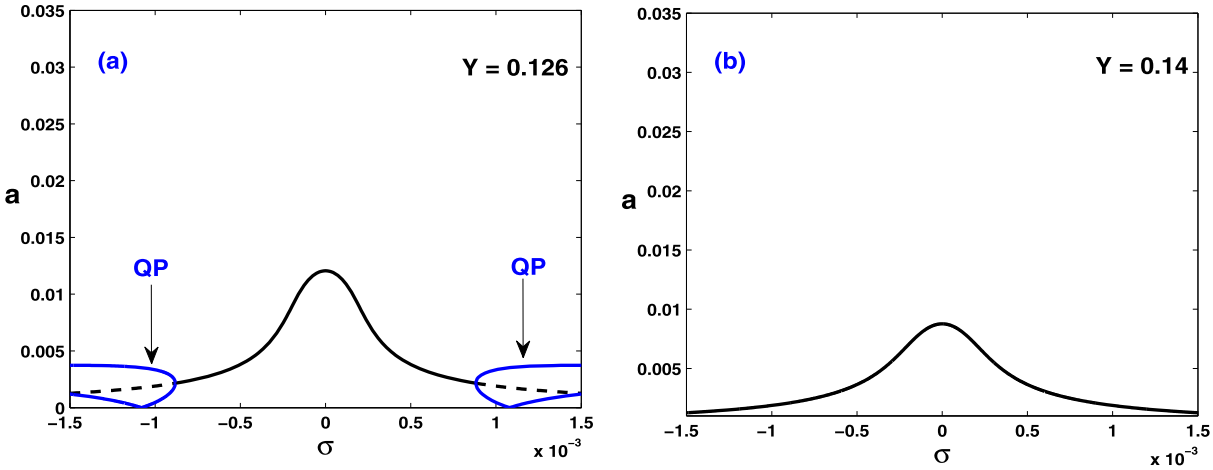

Fig. 7 Periodic and QP galloping versus σ for the parameter values of Fig. 5

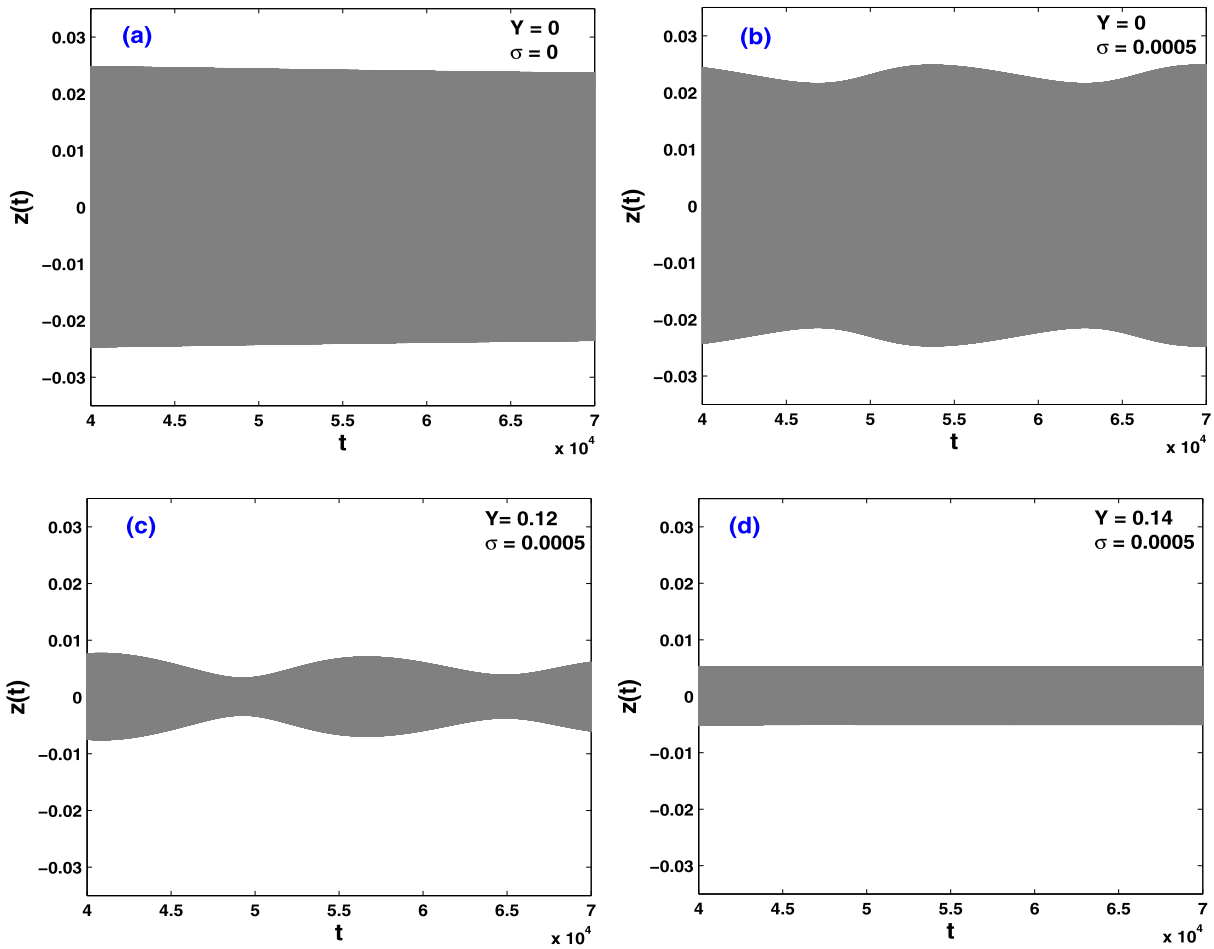

Fig. 8 Examples of time histories of the slow dynamics $z(t)$ for the parameter values of Fig. 5. Values of Y and σ are picked from Figs. 5, 6, and 7b

serves that in the absence of the FHE ($Y = 0$) the domain of periodic galloping decreases with increasing V (Fig. 10a) and increases with Y (Fig. 10b), which is coherent with Fig. 6.

4.2 Case of turbulent wind with parametric excitation

In the case of parametric excitation ($u_1 = 0$, $u_2 \neq 0$), Figs. 11a, 11b show the periodic amplitude and the envelope of the QP oscillations for two different values of the amplitude Y. The analytical predictions (solid lines) and the numerical simulations obtained by using Runge–Kutta method (circles) are plotted for validation. The effect of the amplitude Y on the QP envelope is shown in Fig. 11c. One observes that the QP envelope and its mean amplitude decrease substantially with increasing Y, while the interval of the QP response remains constant.

Examples of time histories of the slow dynamic $z(t)$ are shown in Fig. 12 for some values of Y picked from Fig. 11. Figures 12a, 12b show for $\sigma = 0$ and $\sigma = 0.001$, respectively, the periodic and the QP responses in the absence of the FHE. The QP responses are shown in Figs. 12c, 12d for two values of Y confirming the decreasing in the mean amplitude and in the QP envelope, as indicated in Fig. 11c.

Figure 13a shows, in the absence of the FHE, the QP galloping amplitude versus the wind velocity V for a given value of the excitation u_2. It can be seen that as V is increased from zero, the QP galloping appears directly from the rest position with a small modulation and increases with the wind velocity. The small boxes

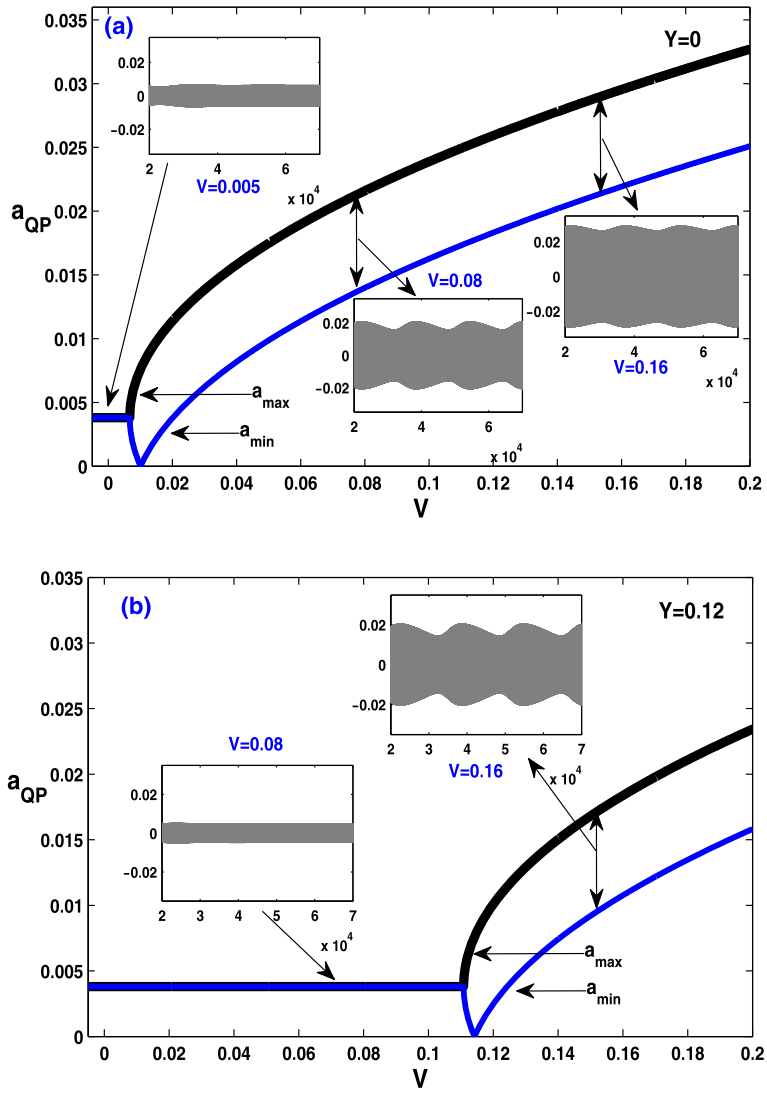

Fig. 9 The QP envelope versus V for the parameter values of Fig. 5 with $\sigma = 0.0005$

inset the figure show time histories of the slow dynamic $z(t)$ for two different values of V. For $Y = 0.12$ and a given value of V, Fig. 13b depicts the QP galloping amplitude and a time history inset the figure showing that a significant retarding of the QP galloping onset can be achieved by increasing the amplitude Y, as clearly shown in Fig. 14.

It is worth noticing that the frequency modulation produced by the parametric excitation (see time histories inset Fig. 13) is higher than the frequency modulation produced by the external excitation (see inset Fig. 9). This result is consistent with the expression of the frequency λ of the QP modulation given by (16), which depends effectively (to the leading order) on the amplitude of the parametric excitation u_2.

In Fig. 15, we show the curves delimiting the regions of periodic (hatched) and QP galloping (unhatched), as given by (23). One observes that the domain of periodic galloping remains constant with increasing V (Fig. 15a) and almost constant as Y increases (Fig. 15b), which is also coherent with Fig. 11c.

Figure 16 illustrates the effect of the amplitude of the FHE on the QP galloping domain in the parameter plane u_2 versus σ_c. The plots show that the QP galloping domain decreases rapidly with u_2 and slightly with Y.

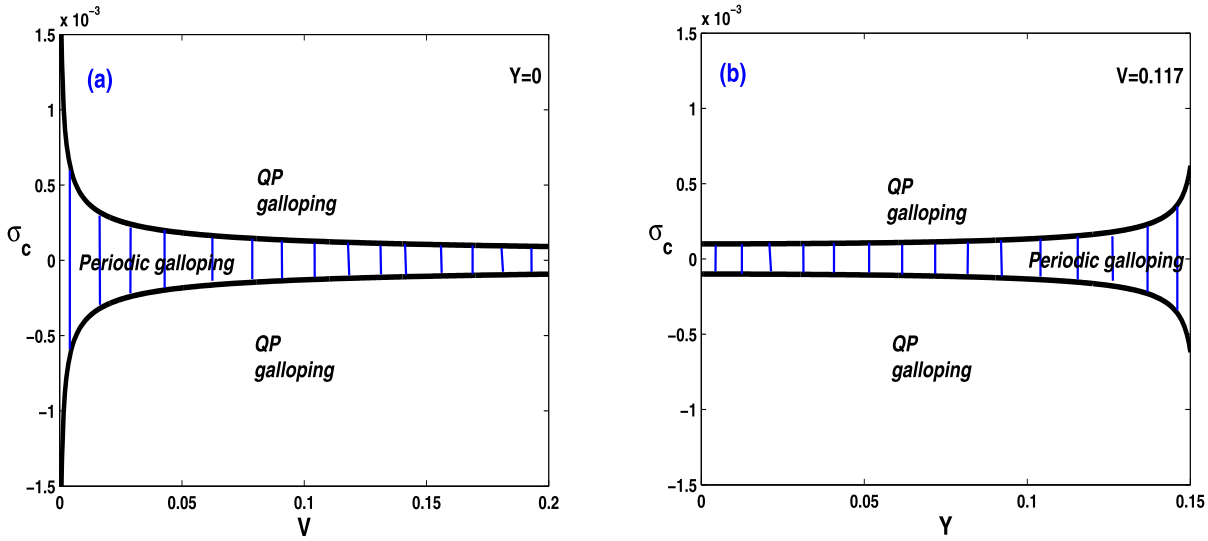

Fig. 10 Periodic and QP galloping domains for $u_1 = 0.033$

Figure 17 shows the effect of the unsteady wind components u_2 on the frequency λ of the QP modulation, as given by Eq. (16). Inspection of this figure indicates that in the case of parametric excitation ($u_2 \neq 0$) the frequency λ decreases rapidly with u_2. The decreasing of λ is more pronounced as the amplitude Y is increased. Notice that in the case of external excitation ($u_1 \neq 0$), the frequency λ remains unchanged (to the leading order) as shown in the figure by the horizontal line.

To support the predicted results shown in Fig. 17, examples of time histories of the slow dynamic $z(t)$ are given in Fig. 18 in the absence of the FHE for values of the unsteady components picked from Fig. 17. Figures 18a, 18b show the QP response in the presence of external excitation ($u_1 \neq 0$), while Figs. 18c, 18d illustrate the QP response in the presence of parametric excitation ($u_2 \neq 0$). It can be clearly seen the significant influence of the parametric excitation on the frequency of the modulation.

4.3 Case of turbulent wind with external and parametric excitations

In the case where turbulent wind activates both external and parametric excitations ($u_1 \neq 0$, $u_2 \neq 0$), Figs. 19a, 19b show the periodic amplitude and the QP modulation envelope in the absence and presence of the FHE, respectively. These figures indicate that increasing the amplitude of the FHE Y eliminates the loop in the amplitude response (as mentioned in Sect. 3) and gives rise to a small new QP modulation envelope emanating from the original QP envelope. The effect of the amplitude Y on the original QP envelope is illustrated in Fig. 19c showing that the mean amplitude as well as the envelope of the QP response decrease while the QP envelopes move away from the resonance generating the new small QP modulation domain delimited by the two thick lines.

Figure 20 shows examples of time histories of the slow dynamic $z(t)$ for some values of Y picked from Fig. 19. Figures 20a, 20b show for $\sigma = 0$ and $\sigma = 0.001$, respectively, the periodic and the QP responses in the absence of the FHE ($Y = 0$). The QP response corresponding to the new born small QP modulation envelopes are shown in Figs. 20c, 20d for a given Y and for two values of σ, confirming the birth of such a new QP modulation envelope.

Figure 21a shows, in the absence of the FHE, the (original and new) QP modulation envelopes versus the wind velocity V for given values of excitations u_1, u_2. One notices that as V is increased (Fig. 21b), the original QP galloping onset increases with the wind velocity while the small envelope persists prior to the original QP galloping envelope QP as shown in the left box inset Fig. 21b. Figure 22 clearly confirms the significant retarding of the large original QP galloping onset by increasing the amplitude Y. One notices that

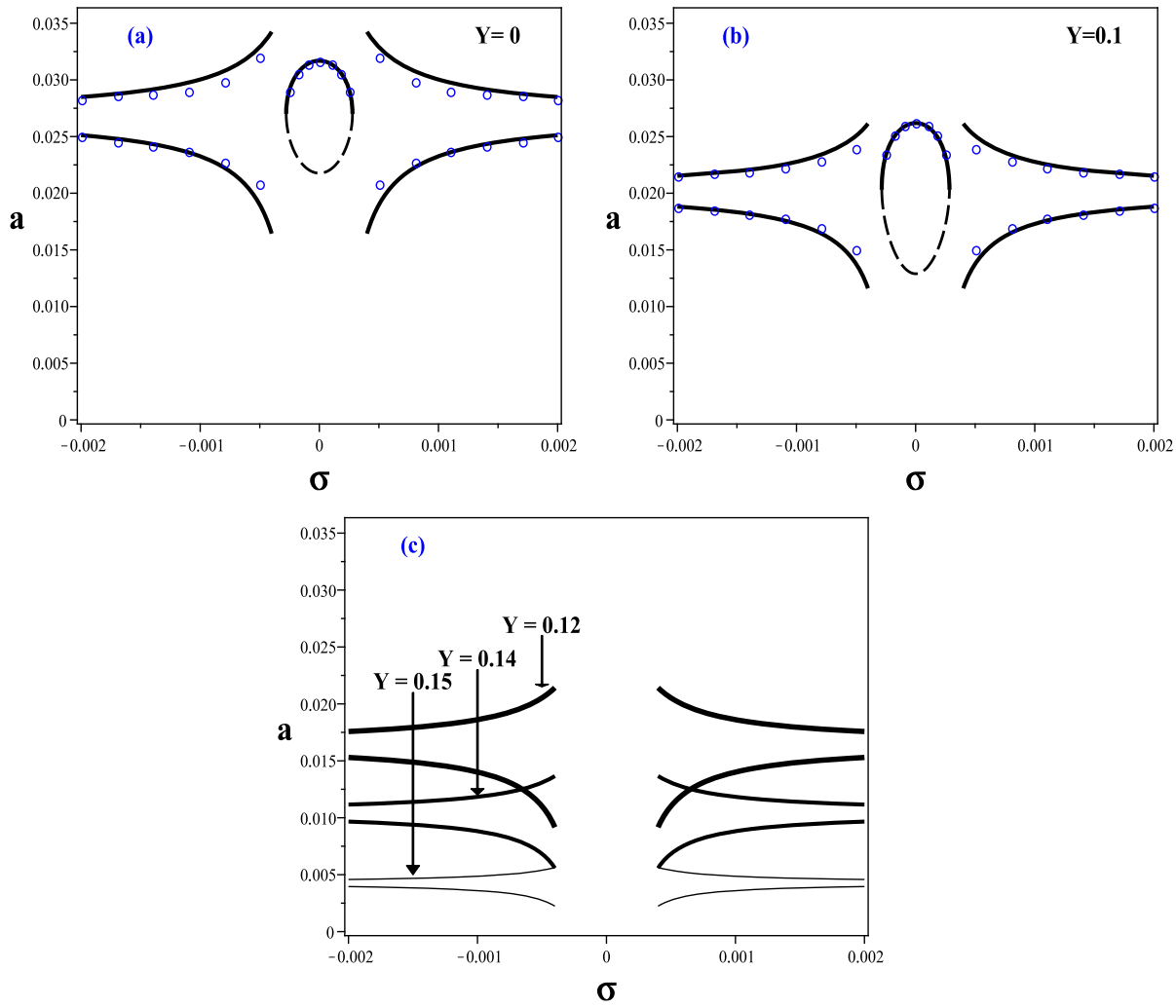

Fig. 11 Amplitude versus σ for $V = 0.167$ and $u_2 = 0.1$

the presence of the new small QP modulation envelope causes the tower to undergo small QP vibrations even in the presence of small wind.

5 Conclusion

The effect of a FHE on the periodic and QP galloping of a tower subjected to steady and unsteady wind was studied analytically near the primary resonance. A lumped mass sdof model was considered and attention was focused on the case where the turbulent wind activates either external excitation, parametric one or both. The TSPA is performed to obtain explicit relationships of the QP responses and the QP modulation envelopes.

In the case of steady wind, the FHE amplitude causes the Hopf bifurcation location to shift toward higher wind velocity, thereby retarding the periodic galloping onset.

In the case of turbulent wind with external excitation and in the absence of the FHE, the tower may experience small periodic response even for very small values of wind velocity, and as the wind velocity increases slightly, small modulation of the amplitude of the periodic response appears causing QP galloping. In the presence of FHE, the QP galloping onset can be retarded keeping the tower oscillating periodically in a large interval of the wind velocity.

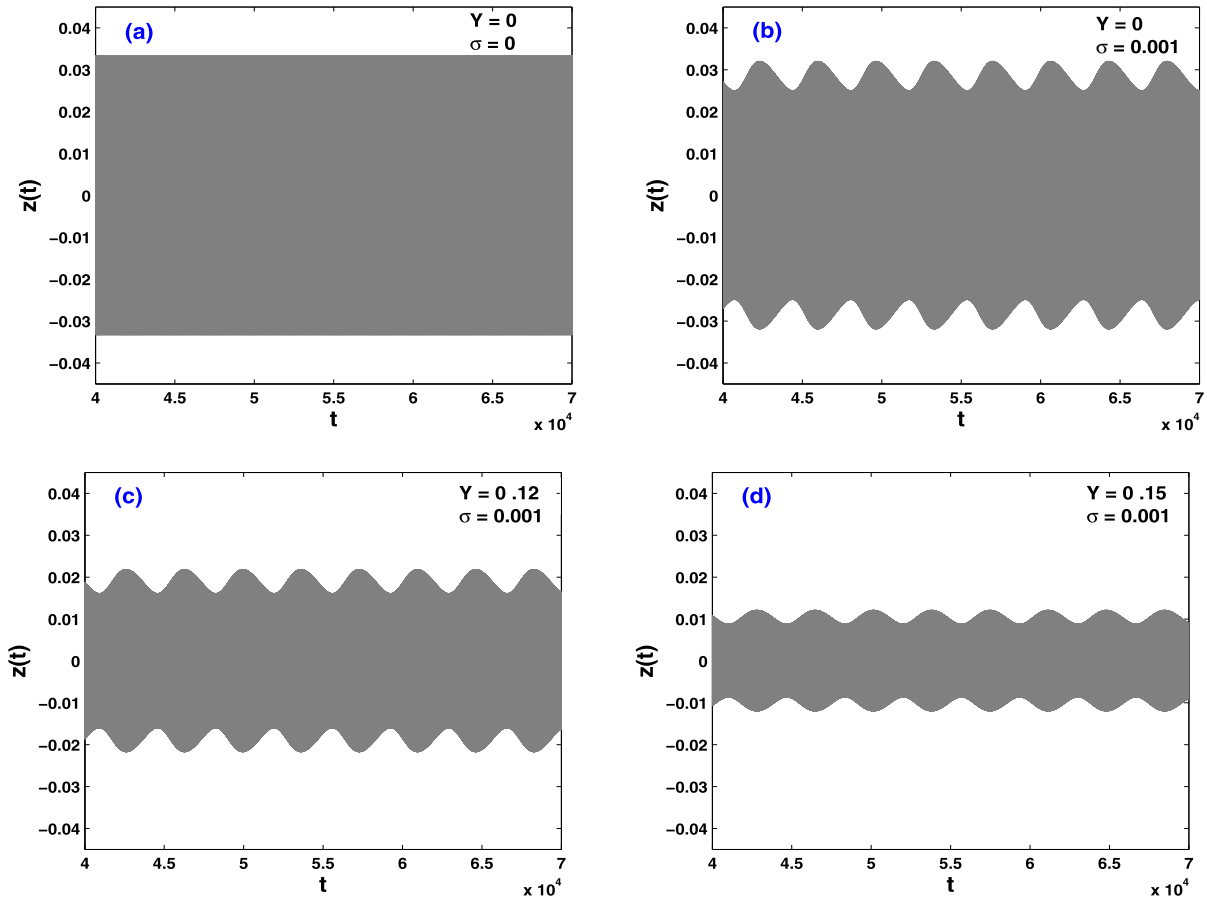

Fig. 12 Examples of time histories of the slow dynamics $z(t)$ for the parameter values of Fig. 11 with $\sigma = 0.0005$. Values of parameters Y and σ are picked from Fig. 11

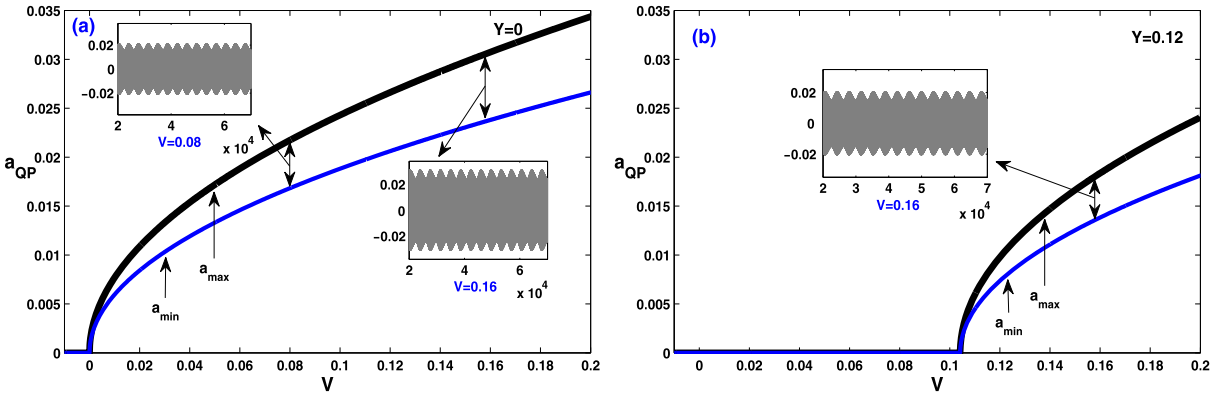

Fig. 13 The QP envelope versus V for the parameter values of Fig. 11 with $\sigma = 0.001$

In the case where turbulent wind activates parametric excitation and in the absence of the FHE, the envelope of the QP galloping with a small modulation appears directly from the rest position which increases with the wind velocity. As the FHE is introduced, the QP galloping onset is significantly

delayed. Moreover, in the case of parametric excitation, the tower develops QP galloping with a higher frequency modulation, compared to the case for which the turbulent wind activates external excitation.

In the case where both external and parametric excitations are activated the FHE eliminates bistability phenomenon, which is responsible for instability and jumps in the amplitude response of the tower.

One can conclude from this work that the effect of wind speed on the onset of QP galloping should not be neglected. Indeed, QP galloping is more likely to occur in large interval of frequencies and then its onset has to be taken into consideration in the design process of tall buildings to enhance stability performance.

The use of FHE may be viewed as a possible alternative control strategy able to retarding the onset of periodic and QP galloping of towers. Such a control can be exploited especially when other strategies, such as mass tuned dampers and tuned liquid dampers, which are often need large places to be installed, cannot be implemented for preventing or retarding large structural vibration.

Finally, it should be noted that the innovative idea of using FHE for retarding galloping onset of tall

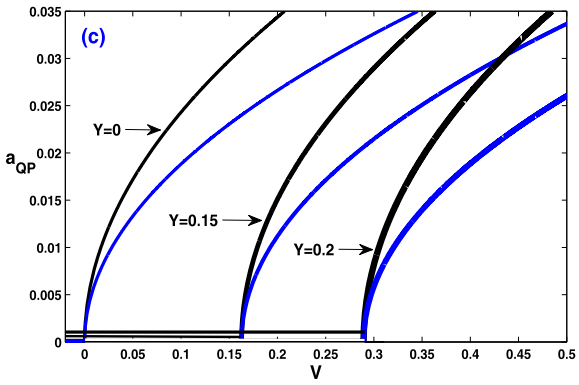

Fig. 14 Effect of Y on the QP envelope for the parameter values of Fig. 11 with $\sigma = 0.001$

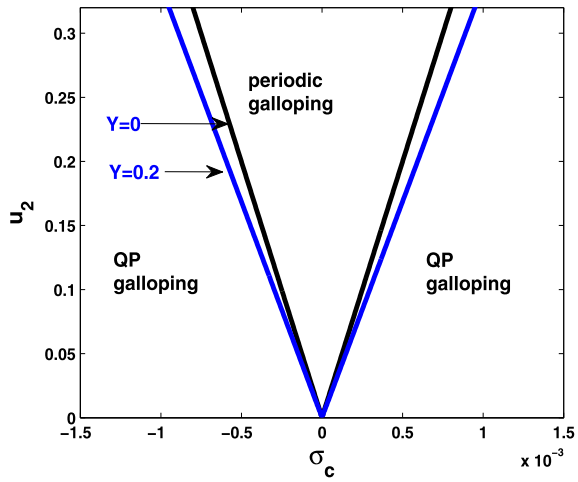

Fig. 16 Periodic and QP galloping domains in the parameter plane u_2 versus σ_c for $V = 0.167$

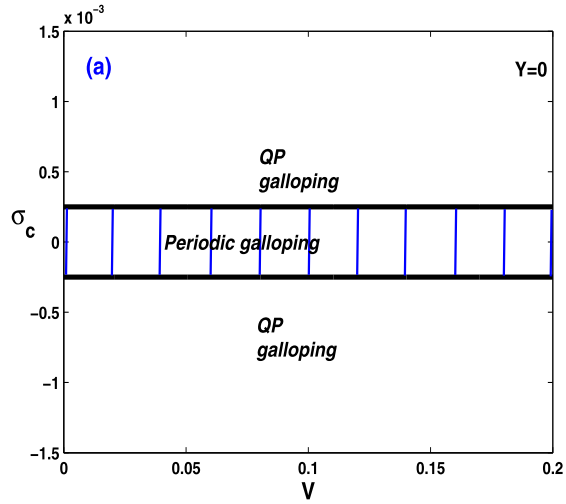

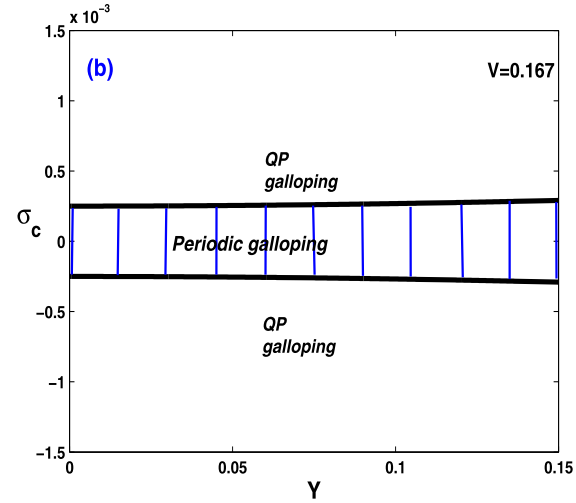

Fig. 15 Periodic and QP galloping domains for $u_2 = 0.1$

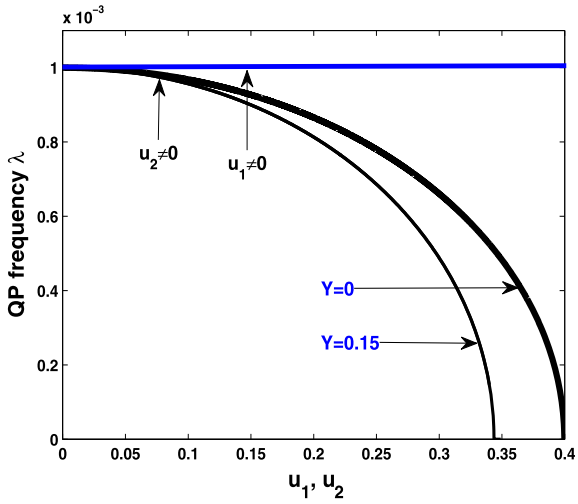

Fig. 17 Variation of the modulation frequency of the QP galloping u_1 and u_2 for $V = 0.167$ and $\sigma = 0.001$

building comes essentially from a previous experimental work on vibrating testing of a full size tower [25]. The mechanical vibration exciter system used in such an experiment was designed so that a sinusoidally varying horizontal excitation can be generated and applied to the tower from the top.

Appendix A

The expressions of the coefficients of Eq. (1) are

$$\omega = \pi \frac{\sqrt{3EI}}{h\ell\sqrt{m}}, \qquad c_a = \frac{\rho A_1 b h \ell \bar{U}_c}{2\pi\sqrt{3EIm}},$$

$$b_1 = c_a, \qquad b_2 = -\frac{4\rho A_2 b \ell}{3\pi m},$$

$$b_{31} = -\frac{3\pi\rho A_3 b \ell \sqrt{3EI}}{8h\bar{U}_c\sqrt{m^3}}$$

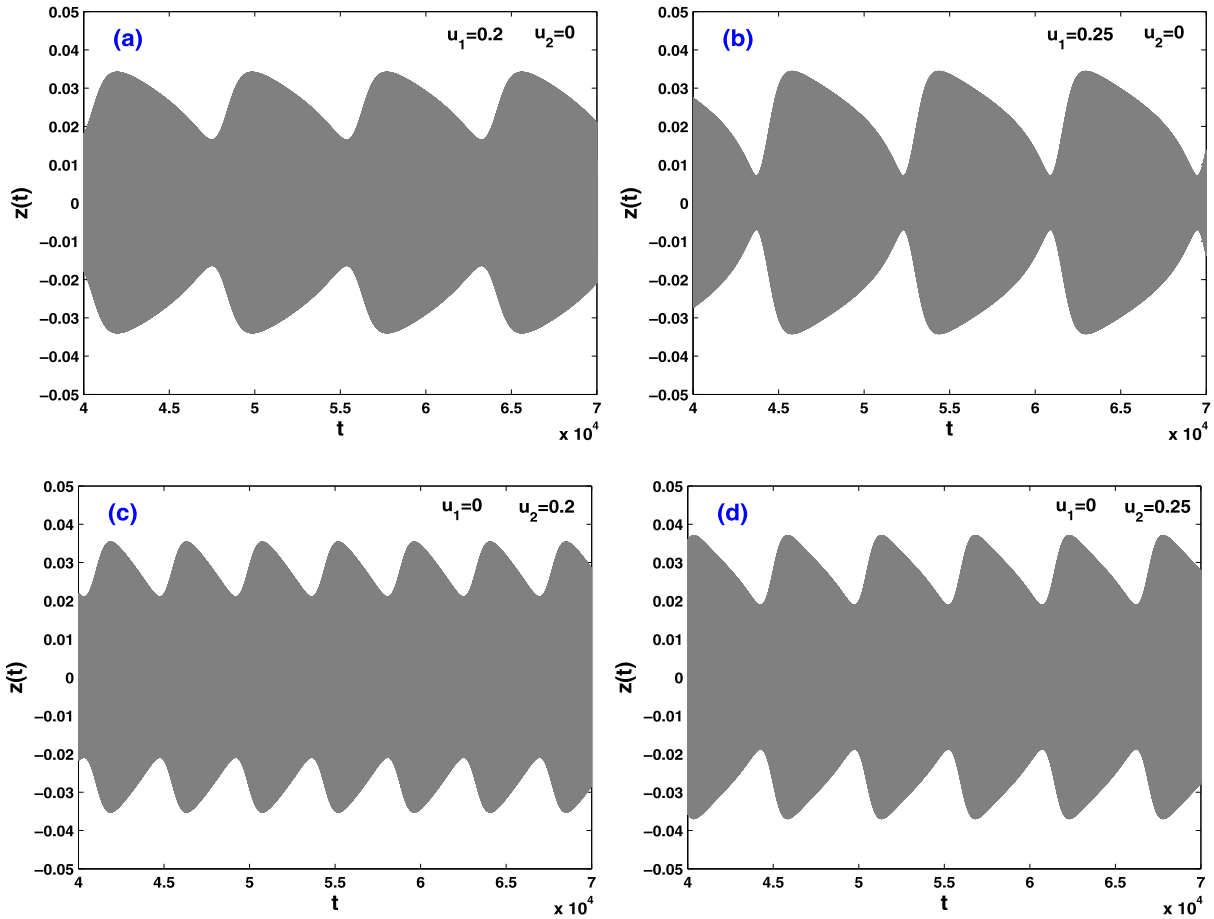

Fig. 18 Examples of time histories of the slow dynamics $z(t)$ for $Y = 0$, $V = 0.167$, and $\sigma = 0.001$

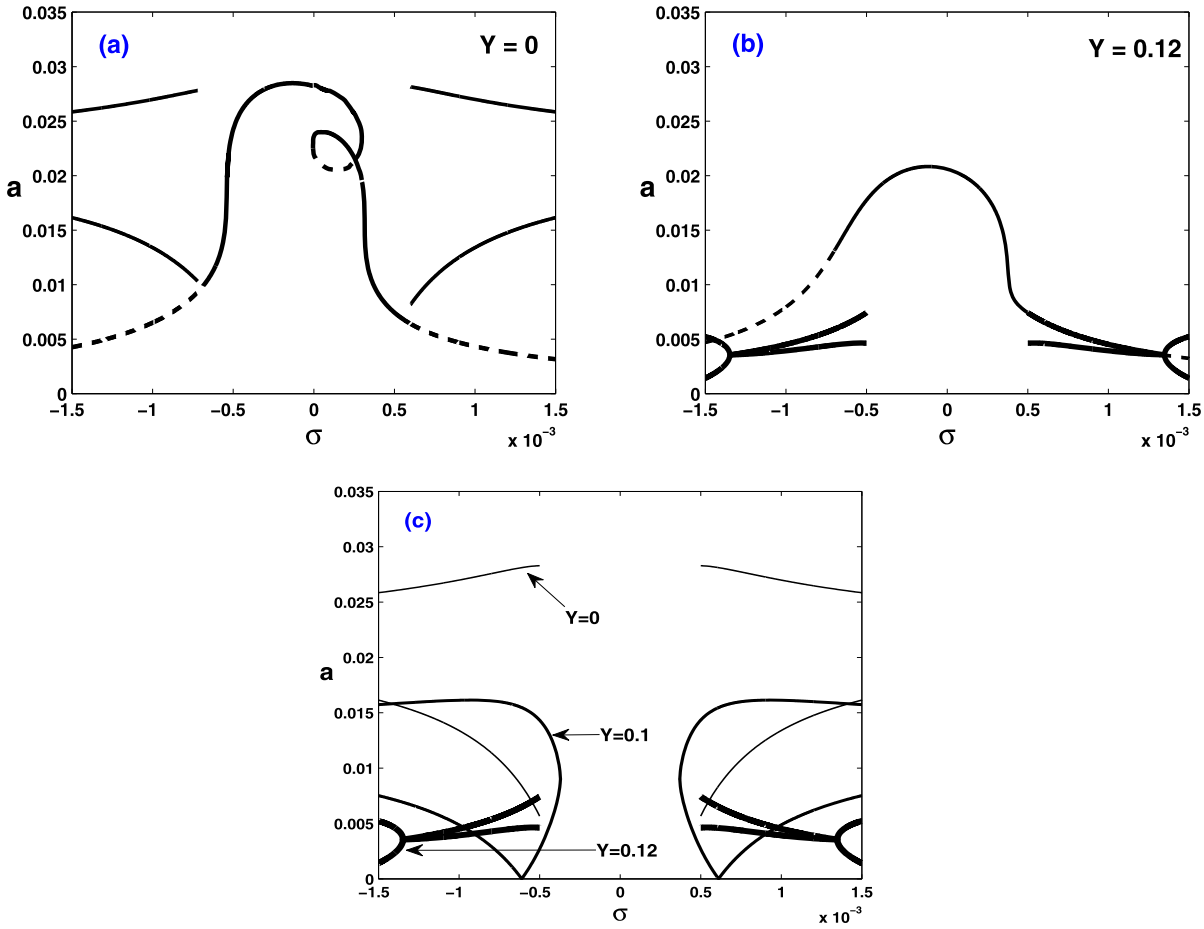

Fig. 19 Amplitude versus σ for $V = 0.11$, $u_1 = 0.1$, and $u_2 = 0.1$. *Thick lines*: new QP modulation envelope

$$b_{32} = -b_{31}, \qquad \eta_1 = \frac{4\rho A_0 b h^2 \ell \bar{U}_c^2}{3\pi^3 EI},$$

$$\eta_2 = \frac{\eta_1}{2}, \qquad U(t) = \bar{U} + u(t),$$

where ℓ is the height of the tower, b is the cross-section wide, EI the total stiffness of the single story, m is the mass longitudinal density, h is the interstory height, and ρ is the air mass density. $A_i, i = 0, \ldots, 3$ are the aerodynamic coefficients for the squared cross-section. The dimensional critical velocity is given by

$$\bar{U}_c = \frac{4\pi\xi\sqrt{3EIm}}{\rho b A_1 h \ell} \tag{24}$$

Here, ξ is the modal damping ratio, depending on both the external and internal damping

$$\xi = \frac{\eta h^2}{24EI}\omega + \frac{c}{2m\omega} \tag{25}$$

The following numerical values picked from [7] are used for convenience: the height of the tower is $\ell =$ 36 m, the cross-section is $b = 16$ m wide, the total stiffness of the single story is $EI = 115318000\ \mathrm{N\,m^2}$, the mass longitudinal density is $m = 4737$ kg/m, the damping ratio is $\zeta = 0.5$ percent (corresponding to $\eta = 128513$ N s, $c = 34.8675\ \mathrm{N\,s/m^2}$ in Eq. (25)). The interstory height is assumed $h = 4m$. The aerodynamic coefficients $A_i, i = 0, \ldots, 3$ are taken from [4] for the squared cross-section: $A_0 = 0.0297$, $A_1 = 0.9298$, $A_2 = -0.2400$, $A_3 = -7.6770$. The air mass density is $\rho = 1.25\ \mathrm{kg/m^3}$. The (dimensional) natural frequency of the rod is $\omega = 5.89$ rad/s. The (dimensional) critical wind velocity assumes the value $\overline{U}_c = 30$ m/s.

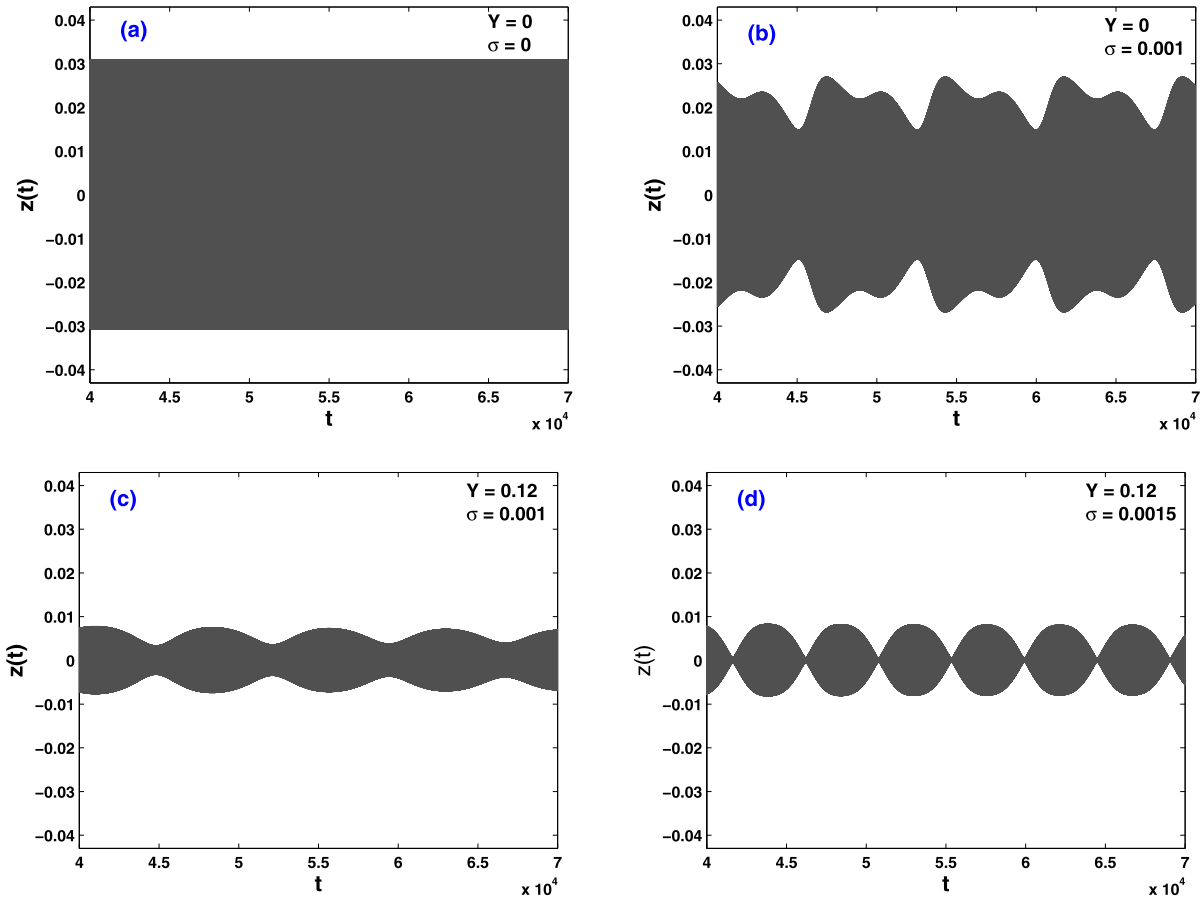

Fig. 20 Examples of time histories of the slow dynamics $z(t)$ for the parameter values of Fig. 19. Values of parameters Y and σ are picked from Fig. 19

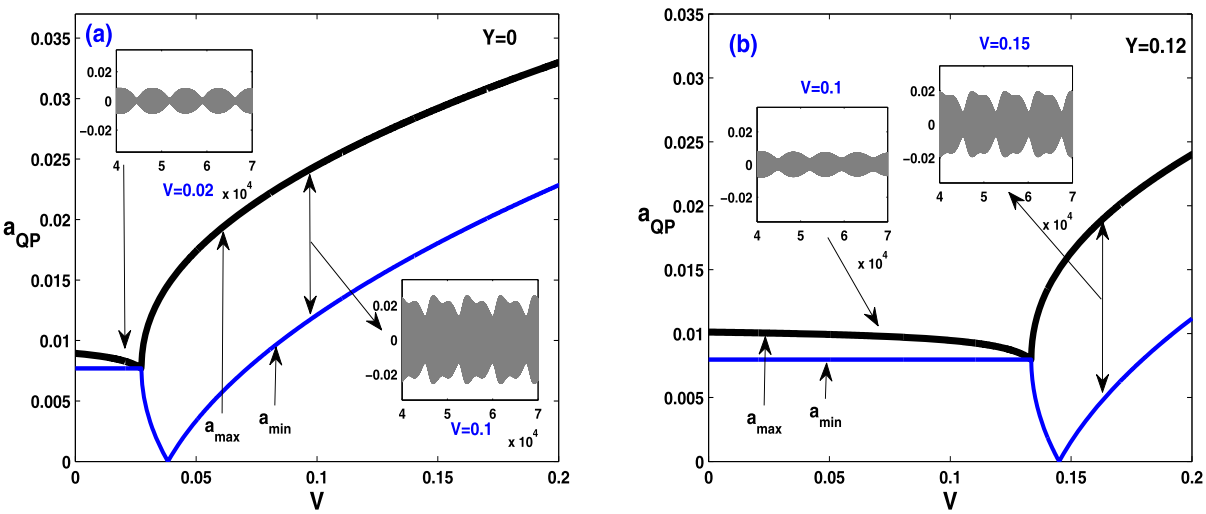

Fig. 21 New and original QP envelopes versus V for the parameter values of Fig. 19 for $\sigma = 0.001$

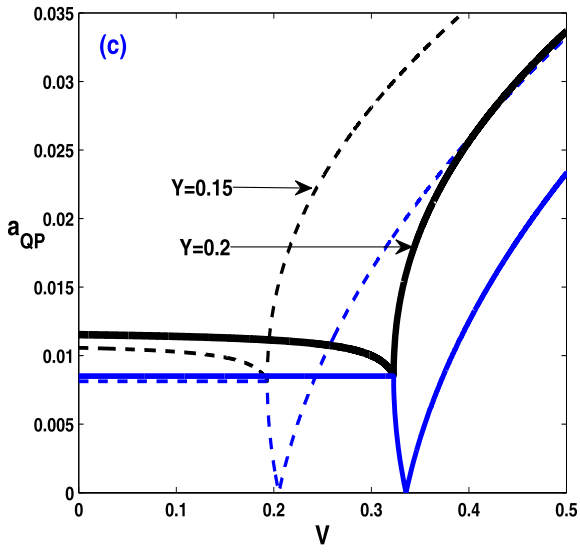

Fig. 22 Effect of Y on QP envelopes for the parameter values of Fig. 19 with $\sigma = 0.001$

Appendix B

Introducing $D_i^j \equiv \frac{\partial^j}{\partial^j T_i}$ yields $\frac{d}{dt} = \nu D_0 + D_1$, $\frac{d^2}{dt^2} = \nu^2 D_0^2 + 2\nu D_0 D_1 + D_1^2$ and substituting Eq. (2) into Eq. (1) gives

$$\begin{aligned}
&\mu^{-1} D_0^2\phi + D_1^2 z + 2D_0D_1\phi + \mu D_1^2\phi \\
&\quad + \big(c_a(1-\bar{U}) - b_1 u(t)\big)(D_1 z + D_0\phi + \mu D_1\phi) \\
&\quad + z + \mu\phi + b_2\big((D_1 z)^2 + 2D_1 z(D_0\phi + \mu D_1\phi) \\
&\quad + (D_0\phi)^2 + 2\mu D_0\phi D_1\phi + (\mu D_1\phi)^2\big) \\
&\quad + \left(\frac{b_{31}}{\bar{U}} + \frac{b_{32}}{\bar{U}^2}u(t)\right)\big((D_1 z)^3 + 3(D_1 z)^2 \\
&\quad \times (D_0\phi + \mu D_1\phi) + 3(D_1 z)(D_0\phi + \mu D_1\phi)^2 \\
&\quad + (D_0\phi + \mu D_1\phi)^3\big) \\
&= \eta_1 \bar{U} u(t) + \eta_2 \bar{U}^2 + Y\cos(\nu t) \qquad (26)
\end{aligned}$$

Averaging (26) leads to

$$\begin{aligned}
&D_1^2 z + \big(c_a(1-\bar{U}) - b_1 u(t)\big) D_1 z + z \\
&\quad + b_2\big((D_1 z)^2 + \langle (D_0\phi)^2\rangle + \langle (2\mu D_0\phi D_1\phi)\rangle \\
&\quad + \langle (\mu D_1\phi)^2\rangle\big) + \left(\frac{b_{31}}{\bar{U}} + \frac{b_{32}}{\bar{U}^2}u(t)\right)\big((D_1 z)^3 \\
&\quad + 3D_1 z\big(\langle (D_0\phi)^2\rangle + \langle (2\mu D_0\phi D_1\phi)\rangle \\
&\quad + \langle (\mu D_1\phi)^2\rangle\big)\big) \\
&= \eta_1 \bar{U} u(t) + \eta_2 \bar{U}^2 \qquad (27)
\end{aligned}$$

Subtracting (27) from (26) yields

$$\begin{aligned}
&\mu^{-1} D_0^2\phi + 2D_0D_1\phi + \mu D_1^2\phi \\
&\quad + \big(c_a(1-\bar{U}) - b_1 u(t)\big)(D_0\phi + \mu D_1\phi) \\
&\quad + \mu\phi + b_2\big(2D_1 z(D_0\phi + \mu D_1\phi) + (D_0\phi)^2 \\
&\quad - \langle (D_0\phi)^2\rangle + 2\mu D_0\phi D_1\phi + (\mu D_1\phi)^2 \\
&\quad - \langle (\mu D_1\phi)^2\rangle\big) + \left(\frac{b_{31}}{\bar{U}} + \frac{b_{32}}{\bar{U}^2}u(t)\right) \\
&\quad \times \big(3(D_1 z)^2(D_0 + \mu D_1\phi) + 3D_1 z(D_0\phi)^2 \\
&\quad - 3D_1 z\langle (D_0\phi)^2\rangle + 6D_1 z\mu(D_0\phi D_1\phi) \\
&\quad + 3D_1 z(\mu D_1\phi)^2 - 3D_1 z\langle (\mu D_1\phi)^2\rangle + (D_0\phi)^3 \\
&\quad + 3\mu(D_0\phi)^2 D_1\phi \\
&\quad + 3D_0\phi(\mu D_1\phi)^2 + \mu D_1\phi\big) \\
&= Y\cos(T_0) \qquad (28)
\end{aligned}$$

Using the inertial approximation [20], i.e., all terms in the left-hand side of Eq. (28), except the first, are ignored, one obtains

$$\phi = -\mu Y\cos(T_0) \qquad (29)$$

Inserting ϕ into Eq. (27), using that $\langle \cos^2 T_0\rangle = 1/2$, and keeping only terms of orders three in z, give the equation governing the slow dynamic of the motion (3).

References

1. Parkinson, G.V., Smith, J.D.: The square prism as an aeroelastic non-linear oscillator. Q. J. Mech. Appl. Math. **17**, 225–239 (1964)
2. Novak, M.: Aeroelastic galloping of prismatic bodies. J. Eng. Mech. Div. **96**, 115–142 (1969)
3. Nayfeh, A.H., Abdel-Rohman, M.: Galloping of squared cantilever beams by the method of multiple scales. J. Sound Vib. **143**, 87–93 (1990)
4. Abdel-Rohman, M.: Effect of unsteady wind flow on galloping of tall prismatic structures. Nonlinear Dyn. **26**, 231–252 (2001)
5. Clark, R., Modern, A.: Course in Aeroelasticity, 4th edn. Kluwer Academic, Dordrecht (2004)
6. Spencer, B.F. Jr., Nagarajaiah, S.: State of the art of structural control. J. Struct. Eng. **129**, 845–865 (2003)

7. Luongo, A., Zulli, D.: Parametric, external and self-excitation of a tower under turbulent wind flow. J. Sound Vib. **330**, 3057–3069 (2011)
8. Tondl, A.: On the interaction between self-excited and parametric vibrations. National Research Institute for Machine Design, Monographs and Memoranda No. 25, Prague (1978)
9. Schmidt, G.: Interaction of self-excited forced and parametrically excited vibrations. In: The 9th International Conference on Nonlinear Oscillations. Application of the Theory of Nonlinear Oscillations, vol. 3. Naukowa Dumka, Kiev (1984)
10. Szabelski, K., Warminski, J.: Self excited system vibrations with parametric and external excitations. J. Sound Vib. **187**(4), 595–607 (1995)
11. Belhaq, M., Fahsi, A.: Higher-order approximation of subharmonics close to strong resonances in the forced oscillators. Comput. Math. Appl. **33**(8), 133–144 (1997)
12. Guckenheimer, J., Holmes, P.: Nonlinear Oscillations, Dynamical Systems, and Bifurcations of Vector Fields. Springer, New York (1983)
13. Nayfeh, A.H., Balachandran, B.: Applied Nonlinear Dynamics: Analytical, Computational, and Experimental Methods. Wiley, New York (1995)
14. Belhaq, M., Fahsi, A.: Analytics of heteroclinic bifurcation in a 3:1 subharmonic resonance. Nonlinear Dyn. **62**, 1001–1008 (2010)
15. Fahsi, A., Belhaq, M.: Analytical approximation of heteroclinic bifurcation in a 1:4 resonance. Int. J. Bifurc. Chaos Appl. Sci. Eng. **22**, 1250294 (2012)
16. Qu, W.L., Chen, Z.H., Xu, Y.L.: Dynamic analysis of a wind-excited stress tower with friction dampers. Comput. Struct. **79**, 2817–2831 (2001)
17. Kirrou, I., Mokni, L., Belhaq, M.: On the quasiperiodic galloping of a wind-excited tower. J. Sound Vib. **32**, 4059–4066 (2013)
18. Belhaq, M., Fahsi, A.: Hysteresis suppression for primary and subharmonic 3:1 resonances using fast excitation. Nonlinear Dyn. **57**, 275–286 (2009)
19. Hamdi, M., Belhaq, M.: Quasi-periodic oscillation envelopes and frequency locking in rapidly vibrated nonlinear systems with time delay. Nonlinear Dyn. **73**, 1–15 (2013)
20. Blekhman, I.I.: Vibrational Mechanics—Nonlinear Dynamic Effects, General Approach, Application. World Scientific, Singapore (2000)
21. Thomsen, J.J.: Vibrations and Stability: Advanced Theory, Analysis, and Tools. Springer, Berlin (2003)
22. Lakrad, F., Belhaq, M.: Suppression of pull-in instability in MEMS using a high-frequency actuation. Commun. Nonlinear Sci. Numer. Simul. **15**, 3640–3646 (2010)
23. Nayfeh, A.H., Mook, D.T.: Nonlinear Oscillations. Wiley, New York (1979)
24. Zulli, D., Luongo, A.: Bifurcation and stability of a two-tower system under wind-induced parametric, external and self-excitation. J. Sound Vib. **331**, 365–383 (2012)
25. Keightley, W.O., Housner, G.W., Hudson, D.E.: Vibration tests of the Encino dam intake tower. California Institute of Technology, Report No. 2163, Pasadena, California (1961)
26. Belhaq, M., Houssni, M.: Quasi-periodic oscillations, chaos and suppression of chaos in a nonlinear oscillator driven by parametric and external excitations. Nonlinear Dyn. **18**, 1–24 (1999)
27. Rand, R.H., Guennoun, K., Belhaq, M.: 2:2:1 resonance in the quasi-periodic Mathieu equation. Nonlinear Dyn. **31**, 187–193 (2003)